RMetS

Royal Meteorological Society

The diabatic heat budget of the upper troposphere and lower/mid stratosphere in ECMWF reanalyses

S. Fueglistaler,[a]* B. Legras,[a] A. Beljaars,[b] J.-J. Morcrette,[b]
A. Simmons,[b] A. M. Tompkins[c] and S. Uppala[b]

[a]*Laboratoire Météorologique Dynamique, Ecole Normale Superieure, and CNRS, Paris, France.*
[b]*European Centre for Medium-range Weather Forecasts, Reading, UK.*
[c]*International Centre for Theoretical Physics, Trieste, Italy.*

ABSTRACT: We present an analysis of the diabatic terms in the thermodynamic energy equation from ERA-40 and the ECMWF reanalysis ERA-Interim. We analyse the clear-sky radiative heating, the cloud radiative effects, and the impact from latent heat exchange and mixing. The diabatic heat budget is closed with the calculation of the temperature assimilation increment. The previously noted excessive tropospheric circulation at low latitudes in ERA-40 is also reflected in the diabatic heat budget. The temperature increment acts to cool the excessive model heating. Conversely, ERA-Interim requires heating from the assimilation increment at low latitudes, suggesting too little convection. In the tropical tropopause layer (TTL), both reanalyses show a strong heating from the interaction of clouds with radiation, but lack of reliable independent estimates renders the role of clouds uncertain. Both reanalyses show cooling in the TTL by the assimilation increment, suggesting that the models may overestimate the cloud radiative heating, or that the convective parametrization scheme has difficulties in capturing the thermal effects of deep convection. In the stratosphere, ERA-40 shows unrealistic radiative heating due to problems in the temperature profile. The diabatic heat balance is dominated by the assimilation increment, and the residual circulation is much faster than in ERA-Interim. Conversely, ERA-Interim is better balanced and requires a substantially smaller temperature increment. Its structure and magnitude of radiative heating/cooling at low/high latitudes is quite realistic. Overall, ERA-Interim provides a much improved residual circulation, but uncertainties in the magnitude of terms in particular around the tropical tropopause remain large. Copyright © 2009 Royal Meteorological Society

KEY WORDS   ERA-40; tropical tropopause layer; cloud radiative effects; data assimilation

Received 28 May 2008; Revised 29 September 2008; Accepted 21 November 2008

1. Introduction

One of the most prominent features of the zonal mean structure of the atmosphere is the pronounced upward bulge of the tropopause over the Tropics, rising from typically 10–11 km over the extratropics to about 17.5 km (cold point) over the Tropics, allowing the possibility for quasi-isentropic troposphere–stratosphere exchange (e.g. Holton *et al.*, 1995). The tropical tropopause is also situated several kilometres higher than the typical outflow level of deep convection, with tracers indicating a transition from troposphere to stratosphere (e.g. Folkins *et al.*, 1999) that begins above the level of main convective outflow. This region, also termed tropical tropopause layer (TTL), is also important because of its role in regulating tracer flux (e.g. water vapour or very short-lived species, VSLS) into the stratosphere.

Theoretical understanding of the transition from the thermally direct (the circulation is driven by gradients in heating) tropospheric Hadley–Walker circulation to the

thermally indirect (the circulation is driven by momentum deposition of upward propagating waves) stratospheric Brewer–Dobson circulation is particularly challenging exactly because of its 'transitional' character. Simplifications usually applied for studies of either circulation (e.g Held and Hou, 1980, for the troposphere; Dunkerton, 1978, for the stratosphere) may not apply, as little information exists about the magnitude of terms *a priori*.

Understanding the circulation requires an understanding of the heat budget, in particular the diabatic terms arising from radiation and latent heat release, which are both virtually impossible to measure directly. In the low-latitude upper troposphere/lower stratosphere (UT/LS), at least three very different processes may be important for understanding the circulation: (i) the direct effect (vertical transport and turbulent mixing) of very deep convection, possibly overshooting the level of neutral buoyancy, (ii) the effect of the spatial organisation of tropical deep convection on quasi-stationary wave patterns in the tropical UT/LS (Gill, 1980; Highwood and Hoskins, 1998) and their impact on upwelling in that layer (recently emphasized by Norton, 2006), and (iii) the stratospheric upwelling induced

---

*Correspondence to: S. Fueglistaler, Dept. of Applied Mathematics and Theoretical Physics, University of Cambridge, Cambridge CB3 0WA, UK. E-mail: s.fueglistaler@damtp.cam.ac.uk

by upward-propagating planetary-scale waves in the sub- and extratropics (Haynes *et al.*, 1991; Holton *et al.*, 1995; Plumb and Eluszkiewicz, 1999). Accurate knowledge of the heat balance terms is required to resolve the roles played by these processes.

The purpose of this paper is to draw attention to the (diabatic) terms of the heat balance, and their uncertainties. In doing so, we hope to promote more stringent comparisons among models and observation-based estimates of the heat balance terms. We have chosen to present and document European Centre for Medium-range Weather Forecasts (ECMWF) analysed data rather than a (free-running) atmospheric general circulation model (GCM) or even a coupled chemistry–climate model (CCM) because of the tight constraints placed by the data assimilation on the temperature profile, which in turn is crucial for accurate radiative transfer calculations. Analysis (and reanalysis) data are frequently used to study troposphere–stratosphere exchange (e.g. Sprenger *et al.*, 2003; Schoeberl, 2004; Fueglistaler *et al.*, 2004), to drive chemical transport models for the stratosphere (Monge-Sanz *et al.*, 2008, provides a comparison of results obtained with different ECMWF analyses), to diagnose eddy momentum fluxes (e.g. Trenberth and Stepaniak, 2003), and to document the large-scale circulation (e.g. Dima and Wallace, 2007). The assimilation process, however, is not energy conserving and the model internal heat budget is not necessarily compatible with the circulation imposed by the analysis process, a point we emphasise in this paper. Understanding the role played by the assimilation process remains an area of active research (e.g. Tan *et al.*, 2004; Pawson *et al.*, 2007).

Assessment of the fidelity of the heat balance in a GCM typically occurs through comparison of atmospheric and surface temperature fields, rain rates and surface and top-of-atmosphere radiative fluxes. Agreement of temperature fields with observations, however, does not necessarily imply that the heat budget is correct, as errors in different terms of the heat budget can mutually cancel. In contrast to a GCM, temperature fields in analysis data should by design agree with observations. Errors in the heat budget of analysis data may manifest themselves in the form of assimilation temperature increments.

The broad use of the ECMWF 40-year reanalysis data (ERA-40) renders this dataset attractive as a starting point for a discussion of the heat balance. However, we found that ERA-40 produces very large assimilation increments (further discussed below) and shows unrealistic radiative heating rates particularly at high latitudes. We therefore make use of data obtained from an interim reanalysis run at ECMWF (labelled ERA-Interim), which shows less artefacts due to an improved data assimilation system, a 4-dimensional variational (4D-Var) assimilation scheme, and a generally improved numerical weather prediction model (Simmons *et al.*, 2006; Uppala *et al.*, 2008). We also show data from an experimental reanalysis at ECMWF (called experiment 471, henceforth labelled EXP-471) that also uses a 4D-Var assimilation scheme, but a model version between that of ERA-40 and ERA-Interim. Because of the problems of ERA-40,

we mainly use data from ERA-Interim to document the model diabatic fields. In addition, we show specifically selected data from ERA-40 and EXP-471 to highlight differences between the three models and assimilation products. For radiative heating rates, we also use previously published, independent estimates for comparison. Our analysis primarily focuses on the atmospheric layer from about 300 to 10 hPa at lower latitudes (about 45°S–45°N). However, plots often show larger sections (from Pole to Pole, and down to 500 hPa) in order to set the focus region into the broader context, and we also discuss some of the prominent features outside the focus region (in particular the southern high latitudes).

Section 2 presents the data and methods. Section 3 discusses the annual mean structure of the diabatic model terms, and compares them to independent estimates. Section 4 discusses some aspects of the Quasi-Biennial Oscillation (QBO) on the stratospheric radiative heating structure. Section 5 discusses the impact of the assimilation process on the heat budget of analysed data. Finally, section 6 provides an outlook.

2. Data and method

2.1. ECMWF analysis data

We use analysed data from the ECMWF 40-year reanalysis project ERA-40 (Uppala *et al.*, 2005), an experimental reanalysis run (EXP-471) and a recent interim multi-year reanalysis (ERA-Interim). Table I summarizes key characteristics of these reanalyses; a detailed description of changes between ERA-40 and ERA-Interim is provided by Simmons *et al.* (2006). The model heat budget is determined from the model forecasts at the intermediate time steps 03, 09, 15 and 21 UTC; analysis times are 00, 06, 12 and 18 UTC.

ECMWF provides integrated (over the forecast period) total diabatic heating rates, all-sky radiative heating rates (separated into short- and long-wave components), and clear-sky radiative heating rates. Data were obtained on the 60 model eta levels (sigma levels following orography in the lower troposphere, flattening progressively to become pressure levels in the stratosphere), interpolated onto a 1° × 1° longitude/latitude grid. Prior to calculating time means, the data were linearly interpolated in log-pressure space on fixed pressure levels. In the case of assimilation increments, data were averaged on the model levels and afterwards converted to pressure levels based on time-mean surface pressure fields. Possible implications of this procedure are confined to levels below about 125 hPa.

Note that ERA-40 provides an ozone field that is based on a simplified ozone scheme (Cariolle and Déqué, 1986; Oikonomou and O'Neill, 2006). However, this ozone field is not used for the radiative transfer calculations. (It will be shown below that this ozone field produces unrealistic radiative heating rates.) Instead, all three ECMWF models use a zonal mean, monthly mean ozone climatology (Fortuin and Langematz, 1994; henceforth FL94)

Table I. Set-up of ECMWF reanalyses (see also Simmons *et al.*, 2006).

	ERA-40	EXP-471	ERA-Interim
Period	1958–2002	2000	1989–200(7)
Assimilation	3D-Var	4D-Var	4D-Var
Assimilation cycle	6 hours	12 hours	12 hours
Analysis (UTC)	00/06/12/18	00/06/12/18	00/06/12/18
Heating from[a]	6-hour forecast	12-hour forecast	12-hour forecast
Model cycle	23r4	29	31
Resolution[b]	T159/L60	T159/L60	T255L/L60
LW radiation	RRTM[c]	RRTM[c]	RRTM[c]
SW radiation	4 spectral intervals	6 spectral intervals[d]	6 spectral intervals[d]
Ice particle size	40–130 μm	30–60 μm	30–60 μm
Radiative bias correction	Static	VarBC[e]	VarBC[e]

[a]Diabatic heating is calculated from model forecasts.
[b]Resolution refers to spherical truncation/levels (TXX/LXX).
[c]Rapid Radiative Transfer Model (Mlawer *et al.*, 1997).
[d]Fouquart and Bonnel (1980).
[e]Variational bias correction.

for the radiative transfer calculations. As a consequence, the ECMWF radiative transfer calculations cannot capture the impact of zonally asymmetric ozone concentrations, or the impact of temporally (other than annual) changing ozone concentrations.

2.2. Method

The thermodynamic energy equation in pressure coordinates may be written as (e.g. Equation 3.58 in Peixoto and Oort, 1992)

$$\frac{\partial T}{\partial t} + \mathbf{v} \cdot \text{grad}\, T - \omega\left(\frac{\kappa T}{p} - \frac{\partial T}{\partial p}\right) = \frac{Q}{c_p}, \quad (1)$$

where $\partial T/\partial t$ is the temperature tendency, Q/c_p is the diabatic heating/cooling, $\mathbf{v} \cdot \text{grad}\, T$ is the horizontal advection of temperature (with $\mathbf{v}$ being the horizontal velocity vector $= \{u, v\}$), and $\omega(\kappa T/p - \partial T/\partial p)$ is the vertical advection of temperature (all terms in K per unit time). Note that this formulation does not explicitly account for diffusive and turbulent (mixing) heat transport.

The heat budget may be set in relation to the zonal mean residual circulation using the transformed Eulerian mean (TEM) framework. For the purpose here, namely a discussion of the terms that constitute the diabatic heating term Q/c_p, a formulation such as Equation (1) is sufficient.

In the atmosphere, the diabatic heating term Q/c_p consists mainly of two terms, namely radiative heating/cooling, Q_{rad}/c_p, and latent heat fluxes, Q_{lat}, from phase changes of water. The ECMWF model forecasts store the total diabatic temperature tendency, and the temperature tendency from radiation. Hence, we cannot reconstruct the diabatic term from latent heat exchange alone. Rather, the 'residual' diabatic heating is the sum of latent heat exchange and diffusive and turbulent heat

transport, Q_{mix}/c_p:

$$\frac{Q}{c_p} = \frac{Q_{rad}}{c_p} + \left(\frac{Q_{lat}}{c_p} + \frac{Q_{mix}}{c_p}\right). \quad (2)$$

Note that part of the condensate re-evaporates at upper levels, but generally latent heat release exceeds uptake, and for simplicity we refer here to latent heat release only. The radiative heating term may be further separated into a clear-sky term, Q_{clear} (i.e. radiative transfer calculation performed without clouds) and a cloud term, Q_{cloud}, that provides the modification due to the presence of clouds. Thus we define

$$Q_{all} \equiv Q_{clear} + Q_{cloud}, \quad (3)$$

which we can further separate into long-wave (LW) and short-wave (SW) components, which are stored separately. Note that Q_{cloud} may be non-zero both inside clouds as well as in cloud-free segments of an atmospheric profile due to modified short- and long-wave fluxes arising from clouds above and/or below.

In discussions of the interaction of temperature and radiation we use the Newtonian cooling approximation to allow a qualitative interpretation of the relation between errors in temperature and radiative heating. Newtonian cooling reduces the complex budget of absorption and emission in an atmospheric layer to the form

$$\frac{Q}{c_p} \approx -\alpha * (T - T_{eq}), \quad (4)$$

where T_{eq} is the radiative equilibrium temperature (i.e. the temperature at which absorption equals emission), and α is the inverse of the radiative relaxation time scale $\tau = 1/\alpha$. The Newtonian cooling approximation arises from a linearization of the radiative transfer equation, and is useful for small perturbations in temperature. In this limit, changes in T_{eq} and α are small compared to those

in T, and the perturbation (denoted as primed quantities) in radiative heating is approximately proportional to the perturbation of the layer's temperature, i.e.

$$\frac{Q'}{c_p} \approx -\alpha * T'. \tag{5}$$

That is, a negative temperature perturbation ('colder') leads to larger radiative heating, and *vice versa*. The equilibrium temperature T_{eq} depends on the divergence of incoming radiation, and as such depends also on absorber characteristics and concentrations, with the implication that the impact of tracer perturbations on radiative heating rates can also be qualitatively interpreted as a consequence of a perturbation of T_{eq}, i.e. in analogy to Equation (5):

$$\frac{Q'}{c_p} \approx -\alpha * T'_{eq}.$$

Although useful for our purpose here (to provide a qualitative interpretation of errors in radiative heating), we emphasize that the Newtonian cooling approximation is subject to limitations (e.g. Goody and Yung, 1989), and it should be borne in mind that (i) the approximation as formulated in Equation (5) assumes that the leading-order term affecting radiative heating rates in a given layer arises from the modification of local emission as a consequence of the layer's temperature change, and (ii) T_{eq} and α are not strictly independent, and α has a strong dependence on both absolute temperature and the vertical scale of a temperature perturbations (e.g. Fels, 1982; Bresser *et al.*, 1995).

Finally, in the case of assimilated data, the heat budget is closed by taking into account the assimilation temperature increment between forecast, T_{fc}, and assimilated, T_{assim}, temperature fields, which we may write as

$$\frac{Q_{assim}}{c_p} = \frac{T_{assim} - T_{fc}}{t_{fc}}, \tag{6}$$

where t_{fc} is the forecast period.

Integrating the assimilation increment into the thermodynamic energy equation gives the equation for the combined model and assimilation system. For simplicity, we use finite differences, and combine the advective terms into one term δT_{adv}. Further, we use the superscripts 'm' to denote quantities derived from the model forecast, and 'assim' for quantities arising from the assimilation system. Quantities without superscript refer to the true state. Then, rewriting Equation (1),

$$\delta T + \delta T_{adv} = \frac{\delta Q}{c_p}, \tag{7}$$

and for the model

$$\delta T^m + \delta T^m_{adv} = \frac{\delta Q^m}{c_p}. \tag{8}$$

By definition, the assimilation increment corrects the temperature tendency difference between the true value δT and the model value δT^m,

$$\delta T^{assim} \equiv -(\delta T^m - \delta T) \tag{9}$$

$$= -\left(\frac{\delta Q^m}{c_p} - \frac{\delta Q}{c_p}\right) + (\delta T^m_{adv} - \delta T_{adv}). \tag{10}$$

The total diabatic tendency in the assimilated system is the sum of the model diabatic tendency and the assimilation increment,

$$\delta T^* \equiv \frac{\delta Q^m}{c_p} + \delta T^{assim} \tag{11}$$

$$= \frac{\delta Q^m}{c_p} - \left(\frac{\delta Q^m}{c_p} - \frac{\delta Q}{c_p}\right) + (\delta T^m_{adv} - \delta T_{adv}) \tag{12}$$

$$= \frac{\delta Q}{c_p} + (\delta T^m_{adv} - \delta T_{adv}). \tag{13}$$

Hence, we see that the total diabatic tendency is independent of model errors in the diabatic terms, and that δT^* recovers the true diabatic heating in the absence of errors in the advective terms (i.e. for $\delta T^m_{adv} = \delta T_{adv}$). However, the same is not true for errors in the advective terms. In this case, the total diabatic heating δT^* recovers the diabatic heating required to sustain the circulation (and associated heat fluxes) as enforced by the wind and temperature fields. Note that errors in the advective terms may arise from errors both in the wind fields (horizontal and vertical) and temperature field imposed by the assimilation system, a point we will return to below.

2.3.   Radiative transfer calculations

The radiative heating rates from the ECMWF models (Morcrette, 2002) are compared to independent radiative transfer calculations using the model of Fu and Liou (1993). The purpose of this comparison is not to determine whether one of the two models is better, but to provide a sense of the level of agreement of radiative heating rates obtained from two different state-of-the-art radiative transfer models, and for the uncertainty arising from small differences in the tracer concentration profiles, and cloud radiative properties.

In order to compare clear-sky radiative heating rates, we use temperature and tracer profiles obtained from a subset of stations from the Southern Hemisphere Additional Ozone soundings (SHADOZ) program (Thompson *et al.*, 2003). (The stations used were Ascension, Fiji, Java, Malindi, Nairobi, Natal, Paramaribo, Samoa and San Cristobal.) Only profiles extending up to at least 30 hPa were used. Above, profiles were extended up to 0.1 hPa using ECMWF temperature and ozone data. The stratospheric water vapour profiles are based on a climatology from Halogen Occultation Experiment (HALOE) observations. Results discussed here are not overly sensitive to either the stratospheric water vapour profile, nor the vertical extention to 0.1 hPa, but results are shown only up to 30 hPa where the ozone profile is given by the SHADOZ measurements. No correction was applied to upper-tropospheric humidity from the sondes (which

may underestimate water vapour concentrations) other than eliminating (rare) cases of supersaturation.

The impact of clouds on radiative heating rates is compared to previously published estimates based on observed cloud fields. Corti *et al.* (2005) estimated tropical mean, annual mean cloud radiative heating based on cloud field reconstructions derived from a combination of data from the International Satellite and Cloud Climatology Project (ISCCP) and the Lidar in Space Technology Experiment (LITE; Winker and Trepte, 1998). Note that the short duration of the LITE experiment does not allow an 'annual mean' estimate without assuming that the cloud distribution during the observation period is representative for all seasons, which is not the case (e.g. thin cirrus cloud distributions shown by Wang *et al.*, 1996; Spang *et al.*, 2002).

We further make use of the radiative transfer calculations of cloud radiative effects published by Fueglistaler and Fu (2006). Their calculations are based on temperature and humidity soundings and millimetre cloud radar cloud retrievals from the Atmospheric Radiation Measurement (ARM) programme at the tropical Western Pacific locations Manus and Nauru. These calculations represent true annual means (here for the year 2000) for locations of frequent deep convection, but have the disadvantage that they miss the highest, optically thinnest, clouds. The implications of the limitations of these datasets are discussed below.

3. Annual mean model diabatic heating

Figure 1 shows the zonal and annual mean total diabatic heating of ERA-Interim and ERA-40; the same field from EXP-471 (not shown) is similar to that of ERA-Interim. The figure shows strong heating in the tropical troposphere associated with latent heat release. Substantial differences between ERA-Interim and ERA-40 are observed between about 300 and 150 hPa, where ERA-40 shows a much stronger heating and broader region of net diabatic heating than ERA-Interim. At about 150 hPa, both models show a broadening of the diabatic upwelling region, with pronounced maxima of diabatic heating over the subtropics around 70 hPa. Above, ERA-40 shows a narrowing of the upwelling region between about 40 and 20 hPa. In the same layer, ERA-Interim has a broader upwelling region, but also shows a maximum of diabatic heating over the Equator.

Figure 2 shows the zonal mean (left) and equatorial mean (5°S–5°N; right) of clear-sky radiative heating (Figures 2(a, b)), net radiative effect of clouds (Figures 2(c, d)), and 'residual' (Figures 2(e, f)) of the ERA-Interim model for the year 2000. (Adding up these fields gives the total diabatic heating shown in Figure 1(b).)

3.1. Clear-sky radiative heating rates

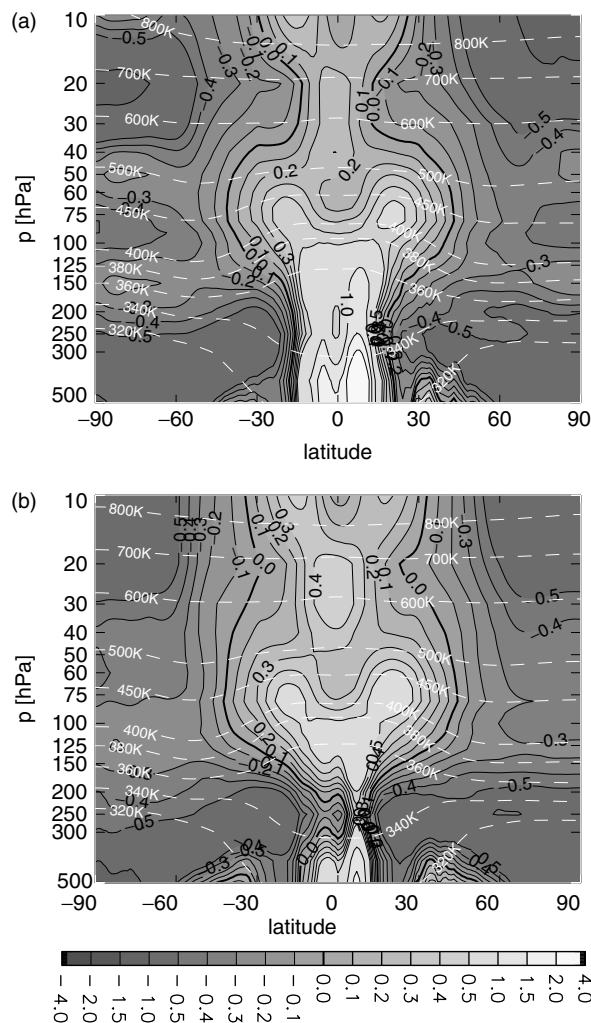Figure 2(a) shows the annual mean (year 2000), zonal mean clear-sky radiative heating from ERA-Interim. The

Figure 1. Zonal mean, annual mean (year 2000) total model diabatic heating rates (grey shading, K day^{-1}; zero line bold) from (a) ERA-40 model, (b) ECMWF interim reanalysis model; white dashed contours show potential temperature (K). Note changes in contour spacing to capture full dynamic range.

figure shows the free troposphere and extratropical stratosphere to be radiatively cooling, and the tropical stratosphere heating. The level of clear-sky zero net radiative heating is located near 125 hPa (about 360 K potential temperature), in agreement with previously published estimates (e.g. Folkins *et al.*, 1999; Gettelman *et al.*, 2004; Fueglistaler and Fu, 2006). In the stratosphere, the latitude where heating turns to cooling is located near 40°, also in agreement with previous estimates (e.g. Rosenlof, 1995).

Figure 2(b) shows the annual mean zonal structure of equatorial clear-sky radiative heating rates. In general, these heating rates are zonally quite uniform. Some zonal asymmetries are found around 200 hPa, and at tropopause levels. While in the troposphere water vapour variations are the likely cause for the asymmetries, the asymmetries at tropopause level arise from the temperature structure. Regions of lowest temperature (for example over the Western Pacific) show largest radiative heating, as expected from the perspective of Newtonian cooling, assuming T_{eq} and α are zonally nearly constant.
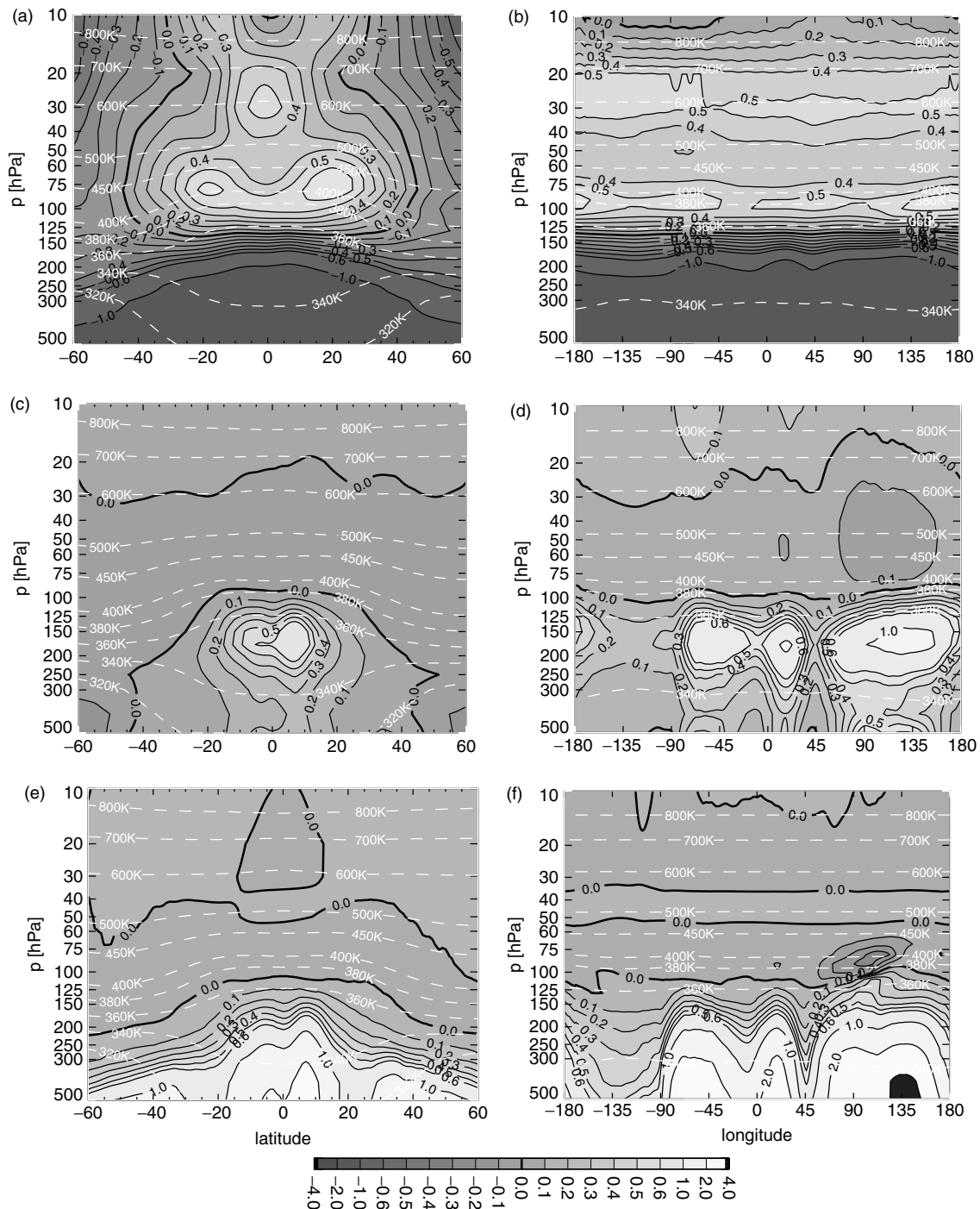
Figure 2. Annual mean clear-sky diabatic heating terms (K day^{-1}) of the ECMWF interim reanalysis model (year 2000). (a) zonal mean versus latitude from 60 °S to 60 °N, and (b) tropical (5 °S–5 °N) mean versus longitude. (c, d) and (e, f) are as (a, b), but for cloud radiative impact, and residual (=latent heat exchange + mixing) terms, respectively. White dashed contours show potential temperature (K). Note changes in contour spacing to capture the full dynamic range.

However, the latter assumption may not be exactly correct because of variations in ozone concentrations which are (positively) correlated with the temperature field. Consequently, the use of a zonal mean ozone climatology in the model may lead to an overestimate of the amplitude of zonal variations of clear-sky radiative heating rates at tropopause levels.

Figure 3 compares profiles of clear-sky radiative heating rates from ERA-Interim, EXP-471 and ERA-40, and radiative transfer calculations as detailed in section 2.3. The panels on the left show tropical (20°S–20°N), annual (2000) and zonal mean profiles of total, short-wave and long-wave radiative heating rates. The three ECMWF calculations are quite similar, except above about 40 hPa where ERA-40 long-wave heating rates are markedly lower than those of ERA-Interim and EXP-471; this difference is also seen in the comparison at the locations of the SHADOZ soundings only (Figure 3(b, d, f)).
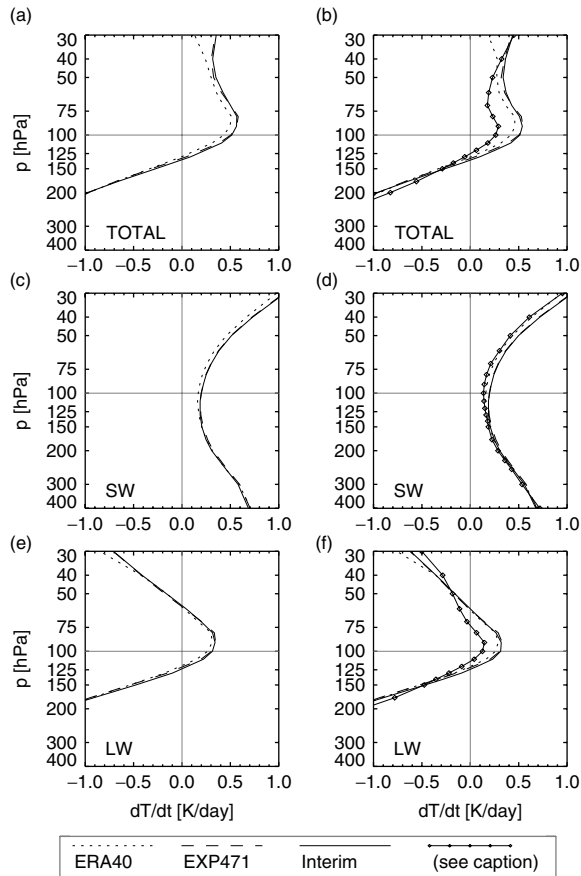
Figure 3. Comparison of annual mean (year 2000) clear-sky total radiative heating rates (K day^{-1}) (a) in the Tropics (20°S–20°N), and (b) at selected SHADOZ stations. (c, d) and (e, f) are as (a, b), but for short-wave and long-wave radiation, respectively. The comparison at selected stations (line with diamonds in (b, d, f)) is based on radiative transfer calculations using the temperature/ozone/water vapour profiles of tropical stations of the SHADOZ program (see text).

Figure 4. ERA-Interim minus ERA-40 for zonal, annual mean (year 2000) (a) temperature (K), (b) short-wave radiative heating (K day^{-1}), and (c) long-wave radiative heating (K day^{-1}). Note change of contour increments at ±0.1 K day^{-1}.

Figure 4(a) shows the zonal mean temperature difference between ERA-Interim and ERA-40, and the differences in all-sky short-wave (Figure 4(b)) and long-wave (Figure 4(c)) radiative heating. The figure shows that, throughout the lower stratosphere at lower latitudes, ERA-40 has higher temperatures than ERA-Interim. Consistent with the Newtonian cooling approximation, the levels with largest temperature difference (e.g. lower latitudes at 30 hPa) have the largest differences in long-wave radiative heating.

Figure 4 further shows that the largest differences in temperatures, and hence in long-wave radiative heating, are found at high latitudes. The ERA-40 temperature profile shows unrealistic oscillations, which give rise to corresponding oscillations in the radiative heating profile.

Conversely, differences in short-wave heating are more uniform between ERA-Interim and ERA-40, except in regions of clouds, where differences are also markedly larger (further discussed below). The differences between ERA-40 and ERA-Interim seen in the stratosphere are related to differences in the short-wave radiative transfer codes of the models (Table I), and to different upwelling short-wave radiation as a consequence of differences in the cloud fields.
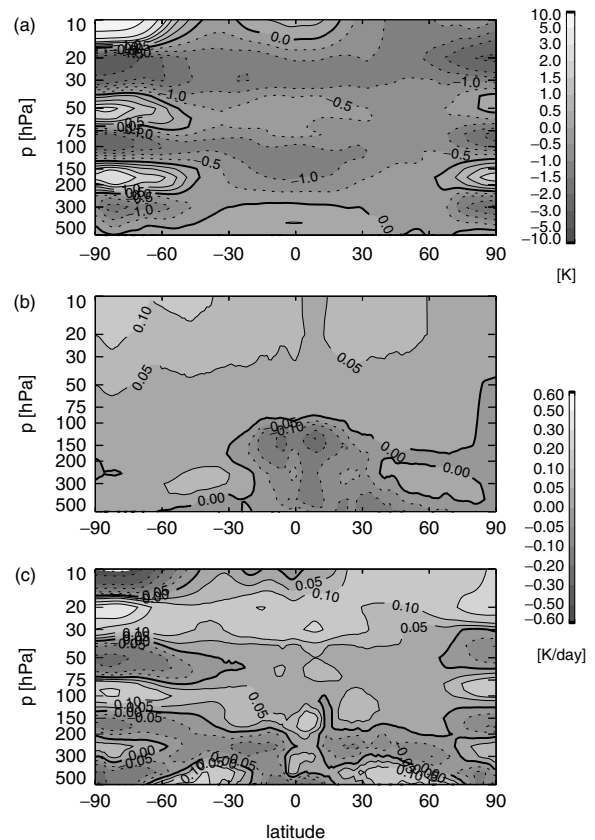
The lower short-wave radiative heating rates of ERA-40 around 30 hPa, combined with the lower long-wave heating rates in that layer due to a warm bias, lead to the 'bottleneck' of model diabatic heating in ERA-40 in that layer (Figures 1(a) and 3). The problem of radiative heating in the stratosphere at low latitudes in ERA-40 becomes particularly pronounced also during periods when the QBO induces a warm anomaly; the role of the QBO is further discussed below. Figure 5 shows the total model diabatic heating of ERA-40 as in Figure 1(a), but for the year 1997. It is readily seen that for this period radiative heating around 20 hPa is negative almost everywhere, which (erroneously) implies that during this period vertical ascent would experience a complete standstill. Were it not for the assimilation increment (discussed below), temperature in this layer would decrease.

The comparison of the clear-sky radiative heating rates from ECWMF and those based on the calculations with the Fu−Liou model at the SHADOZ stations (Figure 3(b)) shows that the shapes of the profiles are similar, but that there are some important differences in magnitude. In particular, the ECMWF profiles have about 0.2 K day^{-1} more heating in the layer 120−60 hPa. Comparison of radiative heating rates between the ECMWF radiative transfer code and the Fu−Liou code based on identical profiles shows generally good agreement, but the Fu−Liou models yields slightly less long-wave heating at tropopause levels of
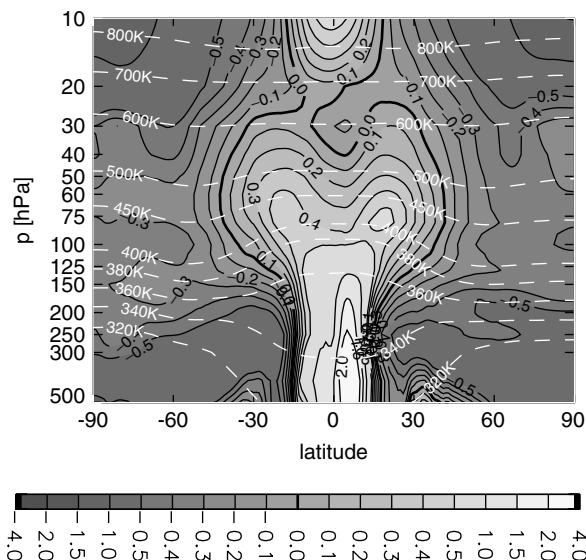
Figure 5. Zonal mean, annual mean (year 1997) total model diabatic heating rates (grey shading, K day^{-1}; zero line bold) from ERA-40 model. White dashed contours show potential temperature (K). This plot may be compared with Figure 1. Note changes in contour spacing to capture full dynamic range.
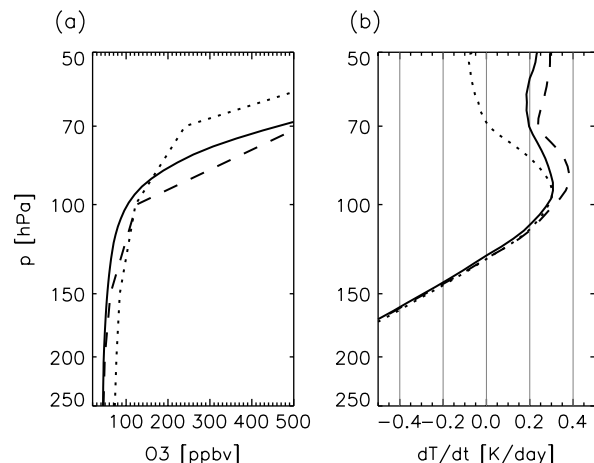

Figure 6. (a) Climatological mean ozone concentrations from SHADOZ (solid), Fortuin and Langematz (1994) at SHADOZ latitudes (dashed) and annual mean (year 2000) ERA-40 ozone field at SHADOZ latitudes (dotted). (b) Corresponding radiative heating rates (assuming diurnal mean insolation) calculated with the Fu–Liou radiative transfer model. (All parameters other than ozone are kept equal.)

about 0.1 K day^{-1} (personal communication S. Tegtmeier and K. Krueger, 2007). Other causes for the differences in the clear-sky radiative heating rates shown in Figure 3 are differing temperature and ozone profiles. We find that the SHADOZ profiles have slightly higher temperature around the tropopause than the ECMWF profiles (which tends to give less long-wave radiative heating; note that this difference may arise from comparing temperatures over different periods, and may not be interpreted as an assessment of the fidelity of temperatures in either dataset), and that the SHADOZ ozone concentrations at tropopause levels are generally lower than those of the FL94 climatology used by ECMWF (which also tends to give less radiative heating).

Figure 6(a) shows the annual mean ozone profile averaged over all SHADOZ stations used here together with the annual mean profile of the FL94 climatology at the latitudes of the SHADOZ stations and the annual mean (year 2000) profile of the ERA-40 ozone field, also at the latitudes of the SHADOZ stations. Figure 6(b) shows that the differences in ozone concentrations translate into substantial differences in radiative heating at tropopause levels and in the lower stratosphere. The higher ozone concentrations of the FL94 climatology account for an increase in radiative heating at tropopause levels of about 0.1 K day^{-1} when compared to the results using the SHADOZ ozone profiles. The figure further shows that using the ERA-40 ozone field (as opposed to the FL94 climatology) gives very unrealsitic radiative heating rates in the stratosphere.

Hence, the difference in clear-sky radiative heating rates between the ECMWF models and the comparison calculation arises from differences of the radiative transfer models and from slightly different temperature and ozone concentration profiles. The difference may

appear small in absolute numbers (about 0.2 K day^{-1} at tropopause levels). However, in relative terms the difference is large, with the ECMWF clear-sky radiative heating being about twice as large as those of the comparison calculation.

3.2. Cloud net radiative heating

Clouds strongly modify absorption and emission, and hence radiative heating rates within the cloud layer. Further, the modification of radiative fluxes leads to effects on heating rates above and below the cloud. Observations indicate a maximum frequency of deep convective cloud occurrence over the Western Pacific warm pool (e.g. Hartmann *et al.*, 2001), and an increase of cloud occurrence frequency in the vicinity of the tropical tropopause with clouds often being optically thin or even subvisible (e.g. Wang *et al.*, 1996). Although optically thin, these clouds are potentially important for the heat budget near the tropopause. Previous model calculations showed that these thin clouds increase radiative heating rates by the order of a few tenths K day^{-1} (with instantaneous heating rates of order a few K day^{-1}), with a corresponding temperature increase of order 1 K (e.g. Jensen *et al.*, 1996; Rosenfield *et al.*, 1998). Recently, Boville *et al.* (2006) reported that a more accurate representation of thin cirrus at tropopause levels helped to eliminate a cold bias in this layer in the Community Atmosphere Model (CAM3). (Note that the main effect is – in terms of the Newtonian cooling approximation – to increase the radiative equilibrium temperature, such that for given upwelling, i.e. constant radiative heating, effective temperatures will be higher).

Figures 2(c, d) show the zonal mean and equatorial mean net cloud radiative effect of ERA-Interim. The overall structure and magnitude of net cloud radiative effect of all three ECMWF models are similar (differences discussed below). The clouds are found to have mostly

a heating effect, that maximizes in the inner Tropics between 200 and 150 hPa, i.e. at the typical outflow level of tropical deep convection. At 100 hPa, the effect is of order 0.1 K day^{-1} and vanishes at the tropopause as there are no further clouds. Not surprisingly, the zonal structure of the cloud radiative effect (Figure 2(d)) follows that of the zonal structure of cloud distribution, with maxima over Southern America, Africa and the Western Pacific warm pool region. In the lower stratosphere, the reduced upwelling long-wave radiation outruns the effect of the increased upwelling (reflected) short-wave flux (Fueglistaler and Fu, 2006, give details), resulting in a net decrease of radiative heating rates over regions of frequent deep convection of order 0.1 K day^{-1}.

Figure 7 shows the net radiative impact of clouds on radiative heating rates of the three ECMWF models, and independent comparison calculations. The figure shows that the shape of the profiles of the three ECMWF models are similar. ERA-Interim shows less net cloud radiative heating around 150 hPa than ERA-40 and EXP-471. The differences are larger for the comparison at selected stations (right panels) than in the tropical mean (left panels), which can be expected for a comparison at single grid points. The decomposition of the total radiative effect into short-wave and long-wave effect (Figures 7(c, e)) of the tropical mean shows that the similar total effect of ERA-40 and EXP-471 actually arises from ERA-40 having larger short-wave heating than ERA-Interim and EXP-471, and EXP-471 having larger long-wave heating that ERA-Interim and ERA-40. At the stations Manus and Nauru, ERA-40 has larger short-wave heating, and ERA-Interim has smaller long-wave heating, than the two other ECMWF models.

The calculations of the net cloud effect by Corti *et al.* (2005) (Figure 7(a)) show a profile markedly different from those of the ECMWF models. Their cloud radiative effect approaches zero at about 150 hPa (data below are not available), whereas all ECMWF models show a net radiative heating of clouds throughout the upper tropical troposphere. Also, their maximum cloud radiative heating (at about 175 hPa) is about a factor of 3 larger than the maximum calculated by Corti *et al.*

The comparison of the cloud radiative heating of ECMWF data with the estimate of Fueglistaler and Fu (2006) over Manus and Nauru shows good agreement up to about 200 hPa. Higher up, the millimetre cloud radar misses optically thin cirrus clouds, and hence tends to underestimate the cloud effect (though one cannot say *a priori* whether this means a negative or positive bias). This clearly limits the conclusions that can be drawn from a comparison in this layer, but we note that the discrepancies are larger for long-wave than short-wave heating. McFarlane *et al.* (2007) report cloud radiative heating of climate models at the ARM TWP stations that are also larger than those derived from a calculation similar to that of Fueglistaler and Fu (2006). At 12 km (about 225 hPa), McFarlane *et al.* (2007) find cloud radiative impacts in models exceeding 1 K day^{-1}, which is even larger than those of the ECMWF models shown here.

Hence, uncertainties regarding the impact of clouds on radiative heating rates are largest between 200 and 100 hPa, where both optically thick anvil clouds as well as thin cirrus clouds occur, which requires a highly accurate reconstruction of the cloud field (vertical profile, diurnal cycle, condensed water content, and optical properties of particles) to accurately calculate its radiative effect.

3.3. Latent heat

Figures 2(e, f) show the annual mean (year 2000) 'residual' diabatic heating rates, calculated as the difference from the total diabatic tendency minus the total, all-sky radiative heating tendency. The resulting quantity represents primarily the net effect of phase changes of water vapour (with latent heat release exceeding latent heat uptake due to evaporation in much of the low-latitude upper troposphere). Further, turbulent mixing (as implemented in the ECMWF models) also contributes to this 'residual' diabatic temperature tendency. The figure shows that latent heat release rapidly decays with height above 200 hPa, and approaches zero around 125 hPa.
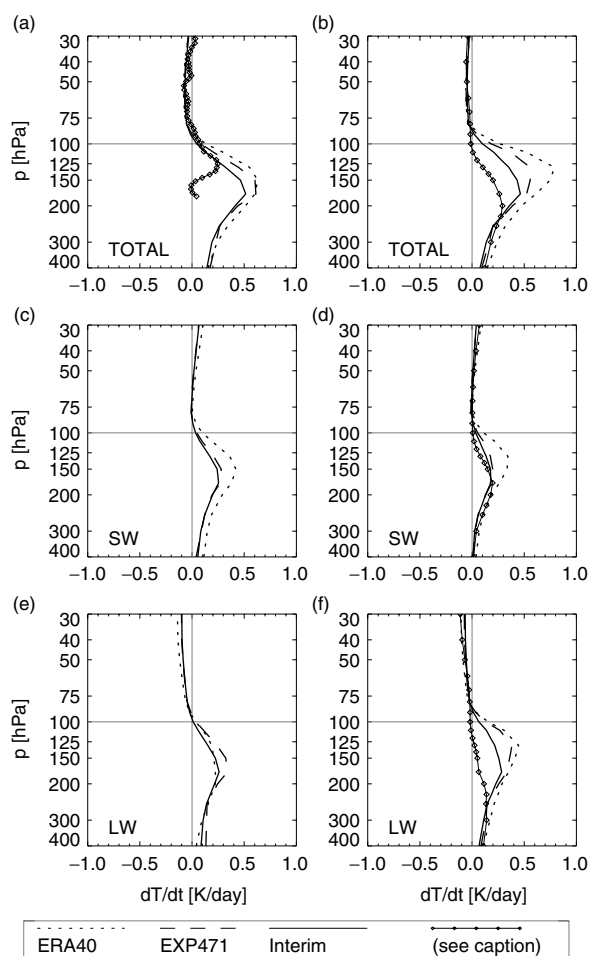

Figure 7. Comparison of annual mean (year 2000) cloud radiative impact (K day^{-1}) (a, c, e) in the Tropics (20°S–20°N, and (b, d, f) at the ARM TWP stations Manus and Nauru. The estimate for tropical mean cloud effect (a; line with diamonds) is adapted from Corti *et al.*(2005); the estimate for cloud effect over ARM tropical western Pacific stations (b,d,f; line with diamonds) is adapted from Fueglistaler and Fu (2006).

The net cooling of the diabatic residual observed west of the dateline just above the tropopause is an unexpected feature that deserves further attention, not least because of ongoing discussions of diabatic subsidence in the stratosphere (Sherwood, 2000; Fueglistaler and Fu, 2006). Inspection of the model data reveals that the model's turbulent mixing parametrization is accountable for the observed diabatic cooling. The vertical mixing induces cooling above (in-mixing of air with lower potential temperature) and warming below (in-mixing of air with higher potential temperature), though the latter is obscured in the time- and zonal-mean view by the contributions from latent heat release. Inspection of instantaneous data (as opposed to the annual mean fields shown here) shows that turbulent mixing is very frequent in the TTL, but that much of its effect averages out over time.

It is difficult to assess whether this mixing is a model artefact or whether it is real. The vertical structure of zonal winds in the assimilated data is probably realistic, and the model's parametrization of mixing based on the Richardson number is physically plausible. It therefore cannot be excluded that the mixing is real, which would bring in a new aspect to the discussion of the heat balance at tropical tropopause levels. According to the model calculations, it constitutes a major heat loss term particularly over the Maritime Continent region where the equatorial easterly jet emanates from the monsoonal upper-level anticyclones. This could provide a simple answer to the puzzle of apparently strong diabatic cooling (the stratospheric 'drain') over this region, without having to invoke convective overshoot (Sherwood, 2000). Note, however, that the amplitude of the cooling is somewhat smaller than reported by Sherwood (2000), and is confined to levels below about 60 hPa.

4. Impact of the QBO

The QBO strongly modulates the structure of radiative heating rates in the stratosphere. Following thermal wind balance, layers with westerly (eastward) wind shear are associated with high temperature anomalies, and layers with easterly (westward) wind shear are associated with low temperature anomalies.

Figure 8(a) shows the inner tropical (10°S–10°N) clear-sky radiative heating rate anomalies for ERA-Interim after subtracting the annual cycle. In the troposphere, interannual variability is mainly associated with ENSO (e.g. the strong El Niño situation in 1998). Closer inspection (not shown) shows that the variations arise from changes in the water vapour and temperature profiles (affecting clear-sky radiative heating rates) as well as from changes in the cloud distribution (affecting the cloud radiative impact, not shown). In the stratosphere, the radiative heating rates show the familiar pattern of downward propagating anomalies associated with the QBO.

The QBO-related variations in stratospheric circulation induce variations in the stratospheric ozone field, which in turn affect radiative heating rates. It is well known
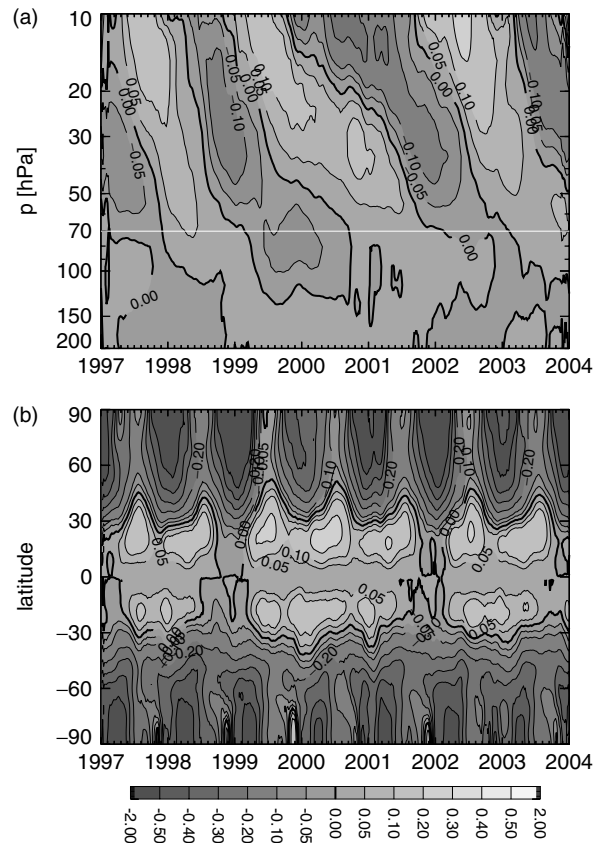

Figure 8. (a) Time series of equatorial (10°S–10°N), interannual (i.e. after subtraction of mean annual cycle) clear-sky radiative heating rate anomalies from ERA-Interim (K day^{-1}). The white line shows the pressure level of the plot in (b). (b) Time series of clear-sky radiative heating rates at 70 hPa after subtracting equatorial values. Note irregular increments for contour lines.

that this feedback plays an important role for the QBO (e.g. Hasebe, 1994). Since the ECMWF radiative heating rates are calculated using a seasonally varying climatological mean ozone field, the model radiative heating rates miss this feedback. Radiative transfer calculations (not shown) using QBO-related ozone variations derived from SAGE II (Stratospheric Aerosol and Gas Experiment) and HALOE (Halogen Occultation Experiment) measurements show, however, that the temperature-dependent variations of heating rates are larger (by about a factor 3) than those arising from the ozone variations. Nonetheless, for model calculations of stratospheric transport that may employ the ECMWF radiative heating rates (as an alternative to the vertical wind field, which is often noisy), this caveat should be borne in mind.

Figure 9 shows the correlation between zonal wind shear over Singapore (as a proxy for the QBO) and the radiative heating rate anomalies at the corresponding pressure surface. The figure shows that westerly (eastward) zonal wind shear over Singapore is associated with negative radiative heating rate anomalies (reduced upwelling) over the inner Tropics (and *vice versa*), in accordance with the expectation from the Newtonian cooling approximation that positive temperatures anomalies in a layer in the tropical stratosphere should be associated with reduced radiative heating rates (and *vice*
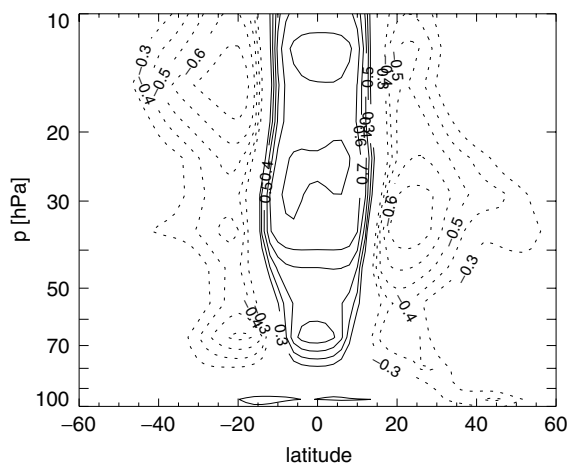
Figure 9. Correlation coefficient of (all-sky) radiative heating rate anomalies (from ERA-Interim) after subtraction of the annual cycle, with zonal wind shear over Singapore, versus pressure level. Equatorial westerly (eastward) wind shear ($du/dz > 0$, $du/d(\ln p) < 0$) is associated with negative heating rate anomalies (reduced upwelling) over the inner Tropics, and enhanced upwelling over the subtropics. Contours show only correlation coefficients ≤ -0.3 and ≥ 0.3.

versa). Further, the figure shows that equatorial westerly wind shear (reduced upwelling) is associated with enhanced upwelling over the subtropics. The radiative heating rate anomalies of the ECMWF reanalyses thus recover the secondary meridional circulation associated with the QBO, and the latitude where the correlation changes sign is consistent with the latitudinal half-width (of order 10°latitude) of the QBO (Baldwin *et al.*, 2001).

The modulation of the latitudinal structure of upwelling by the QBO also plays a role for the prominent 'double peak' structure of radiative heating around 70 hPa (Figure 1). Figure 8(b) shows the time series of radiative heating rates after subtracting the radiative heating at the Equator on the 70 hPa pressure surface. This slightly unconventional calculation highlights the differences between equatorial and off-equatorial heating rates. The figure shows that through much of the period 1997−2003, radiative heating rates at 70 hPa over the subtropics exceed those over the inner Tropics, such that the double peak structure shown in Figure 1 is not a simply because of the particular phase of the QBO in the year 2000. Figure 8(b) shows that only during the progression from low temperature anomaly (easterly wind shear; enhanced equatorial upwelling) to high temperature anomaly (westerly wind shear; suppressed equatorial upwelling), radiative heating rates are uniform over the entire Tropics. (Over the period shown in Figure 8, this situation is found at the beginning of 1997, end of 1998/beginning of 1999, end of 2001/beginning of 2002, and end of 2003.)

The latitudinal structure of stratospheric radiative heating rates provide important constraints and insight into the processes that drive the stratospheric diabatic residual circulation (e.g. Plumb and Eluszkiewicz, 1999). As with the equatorial heating rate anomalies, heating rate variations arising from interannual ozone concentration variations may modify the pattern shown in Figure 8(b). It is clear, however, that the strong modulation of the meridional

structure of radiative heating arising from temperature variations alone calls for some caution with regard to interpretations based on data that may not extend over at least a full period of the QBO. Further, radiative heating rates averaged over the inner Tropics alone (as sometimes seen in the literature) may not be adequate to quantify the diabatic mass flux in the ascending branch of the stratospheric overturning circulation.

Finally, we note that the patterns in clear-sky radiative heating shown in this section are very similar for all-sky calculations, and that clouds have very little impact on interannual variability of stratospheric heating rates.

5. Data assimilation

One of the distinct advantages of assimilated data is that they have relatively tight constraints on the temperature fields, which in turn are critical for accurate calculation of radiative heating rates. However, the assimilation process is not energy conserving (for the atmosphere), and assimilation increments (the difference between model forecast and the final value after assimilation) may arise. The model forecast can produce locally large deviations from the observed state of the atmosphere, for example due to a slight displacement in the forecast of the location of convection or baroclinic instabilities. To first order, the assimilation increment then serves to correct for these errors in the forecast. However, when averaged globally and over time, these forecast errors may be expected to roughly cancel, and the remainder are systematic errors in the model heat budget. The question then is: what kind of errors are these increments correcting?

5.1. Classification of errors

In section 2, we have shown that the assimilation increment corrects for errors in the model diabatic terms, but that errors in the advective terms are not corrected, but compensated. In the latter case, the total diabatic heating does not recover the true diabatic heating in the atmosphere.

Here, we consider it useful to classify errors in the heat budget from the perspective of the model and assimilation system. We distinguish the following types.

(1) Errors that arise from errors in the model itself, for example due to an inaccurate radiative transfer code, or problems with the parametrization of convection. Another prominent example of a type (1) error is lack of an internally generated QBO.

(2) Errors that arise due to incorrect representation of data fields other than wind, whereby we distinguish errors from off-line fields (2a) and errors from assimilated fields (2b). For example, the models discussed here use an ozone climatology to calculate radiative heating rates; an error in this climatology produces an error in the radiative heating rates even if the radiative transfer code is correct, and we would label this error as type (2a). Conversely,

the assimilation process may produce an unrealistic temperature distribution, which again results in incorrect radiative heating rates that we would classify as type (2b) error. The differences in radiative heating rates shown in Figure 4 as a consequence of differing temperature fields would be a good example for a type (2b) error.

(3) Errors that arise because of errors in the dynamical fields (i.e. wind and, coupled via mass conservation, the vertical wind field) that induce spurious heat fluxes.

Note that errors of type (2b) and (3) may result from the assimilation process due to (a) biases in the observations (for example due to radiative effects on radiosonde instruments), and (b) biases arising from the assimilation process itself (of which we will discuss an example in some detail below).

Hence, the interpretation of the assimilation increment is not straightforward, as it may serve to compensate errors in the model physics, or problems associated with the assimilation process. Errors of type (1) and (2) directly affect the model diabatic heating term Q (Equation (1)), and will produce a temperature drift $\partial T / \partial t$ that requires correction by the assimilation. Adding the corrections required to compensate type (1) and (2) errors to the model diabatic heating would greatly improve the model estimate for the true diabatic heating (recall Equation (13)). However, it is virtually impossible to separate type (1) and (2) from type (3) errors. Type (3) errors induce spurious temperature trends via erroneous representation of the *adiabatic* heat flux terms of Equation (1). The correction required by the assimilation in this case would *not* serve to arrive at a correct diabatic heating, but to provide the heating required to compensate the spurious heat fluxes. Hence, it ensures that the erroneous representation of circulation is balanced by the required heating, but does not correct the erroneous circulation towards the true circulation.

Additional constraints are required that can provide clues on the interpretation of the heat budget of an assimilated dataset. In particular, in the absence of a temperature drift of the entire atmosphere over the course of a year, the annual mean diabatic mass flux across an isentropic surface should be zero. This is a *necessary* condition for a correct representation of the atmospheric circulation, but not a *sufficient* condition.

5.2.   Analysis of assimilation increments

Figure 10 shows the annual mean (year 1997, other years are similar) diabatic mass flux integrated over isentropic surfaces calculated from the model (forecast) total diabatic heating, and calculated from the assimilation increment. It is readily seen that the two terms indeed largely cancel, i.e. the global mean assimilation increment on isentropes prevents the model temperatures from drifting. The previously noted underestimation of radiative heating by ERA-40 around 30 hPa (Figure 5) is very evident in Figure 10(a). The large model diabatic heat loss

(dashed line) centred at a potential temperature of about 700 K (corresponding to about 30 hPa) is balanced by a correspondingly large positive assimilation increment (dotted line). Not unexpectedly, the imbalance is larger in the upper troposphere and lower stratosphere (lower plots) than in the stratosphere above. Further, the imbalance is larger (about a factor two) in ERA-40 than in ERA-Interim, which suggests that the model and assimilation process of ERA-Interim are closer to reality.

The figure further shows that the excessive diabatic heating arising from excessive latent heat release in the Tropics in ERA-40 dominates the global balance from 330 to 360 K, such that the assimilation increment has to cool this layer. In other words, the assimilation process acts continously as a heat sink for ERA-40 in that layer. Conversely, ERA-Interim shows too little heating up to 350 K, and the assimilation increment acts as a continous heat source that warms the system in this layer.

Within the expected accuracy, the globally averaged total model heating and assimilation increment compensate each other, except for the region from 350 K to about the tropopause. We have checked for problems arising from numerical inaccuracies (for example due to necessary interpolations), but were not able to identify the cause of the slight imbalance.

The full latitude/height structure of the annual zonal mean assimilation increment is shown in Figure 11 (left column) for ERA-40 (top) EXP-471 (middle) and ERA-Interim (bottom). The right column shows the corresponding total diabatic heating (i.e. total model heating plus assimilation increment). The magnitude of the assimilation increment is by far largest for ERA-40, while EXP-471 and ERA-Interim have similar values. Also, the structure of the assimilation increments in the latitude−height plane of ERA-Interim and EXP-471 is similar. At low latitudes, ERA-Interim and EXP-471 show negative assimilation increments (cooling) between about 200 and 100 hPa, which rises to about 100 to 70 hPa over the subtropics. Further, the assimilation increment is cooling the tropical layer between about 50 and 30 hPa, while the remainder is slightly warmed by the assimilation increment. Common to all three reanalyses (but most pronounced in ERA-40) are oscillations in the vertical structure of the assimilation increment at high latitudes. These oscillations are probably related to the problems of the vertical temperature profile (recall discussion of Figure 4).

The assimilation increment of ERA-40 at lower latitudes shows quite a different structure than ERA-Interim or EXP-471. Up to about 100 hPa, strong cooling is observed throughout the Tropics, followed by strong heating above. The magnitude of the assimilation increment of ERA-40 in particular in the stratosphere is as large, or even larger, than the net model diabatic heating/cooling.

5.3.   Interpretation

Figures 11(b, d, f) show the zonal mean total (i.e. the sum of the model diabatic heating and assimilation
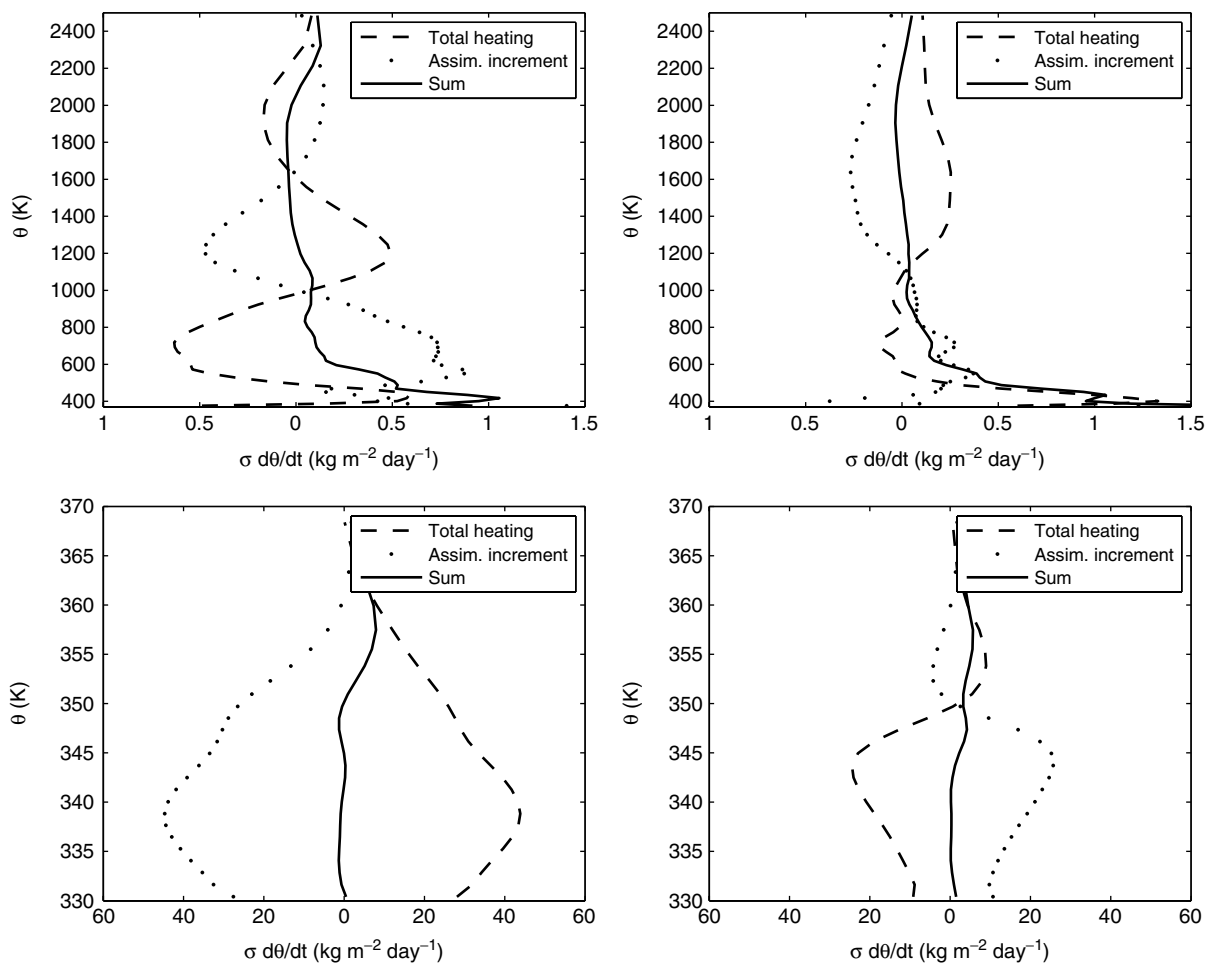
Figure 10. Global average diabatic vertical mass fluxes (year 1997) for ERA-40 (left) and ERA-Interim (right); the vertical profiles are split to accommodate the full range of values. The dashed line denotes the model diabatic cross-isentropic mass flux, and the dotted line the assimilation temperature increment cross-isentropic mass flux. Note that the assimilation increment is expected to balance the imbalance in the model diabatic heating, which is not exactly the case here (see text).

temperature increment) diabatic heating for the year 2000 of ERA-40, EXP-471 and ERA-Interim. We interpret these fields as being the diabatic heating fields corresponding to the residual circulation as represented in each of the reanalysis data. It is readily seen that the total diabatic heating of the three reanalyses are broadly similar inasmuch as they show upwelling at lower latitudes and descent over higher latitudes, but that there are also substantial differences. Since the true atmospheric diabatic heat balance is not known, it is not possible to directly assess the quality of each of the reanalyses. However, combining the information from the model diabatic terms with the assimilation temperature increment, and comparing these terms between the three reanalyses, allows at least a tentative interpretation and assessment.

5.3.1.   The upper troposphere at lower latitudes

Comparison of Figure 1 and Figures 11(b, f) shows that the assimilation temperature increment applied to ERA-40 and ERA-Interim yields convergence for the total (model plus assimilation increment) diabatic heating between ERA-40 and ERA-Interim for this region. For ERA-Interim, the heating provided by the assimilation

temperature increment between 300 and 200 hPa reduces the prominent 'bottleneck' structure (i.e. net heating is confined to a very narrow latitudinal belt just north of the Equator) in the model diabatic heating in this layer (Figure 1(b)). Conversely, the cooling by the assimilation increment between 300 and 100 hPa in ERA-40 reduces the very strong model diabatic heating (Figure 1(a)). The resulting total diabatic heating is more similar than that of the model net diabatic heating. Remaining differences of ERA-40 relative to ERA-Interim are slightly stronger heating just off the Equator, and less heating (in fact cooling) just at the Equator. The total diabatic heating for EXP-471 in this region is about half way between ERA-40 and ERA-Interim.

The fact that all three reanalyses experience cooling from the assimilation increment between 200 and 100 hPa could be seen as an indication for a type (1) error (i.e. an error in the model physics). Possible explanations are that radiative heating in this layer is overestimated by the models. In sections 3.1 and 3.2, we noted that the ECMWF radiative heating arising from clouds appears very large. Also, clear-sky radiative heating at tropopause levels (but not at 150 hPa) was found to be larger than
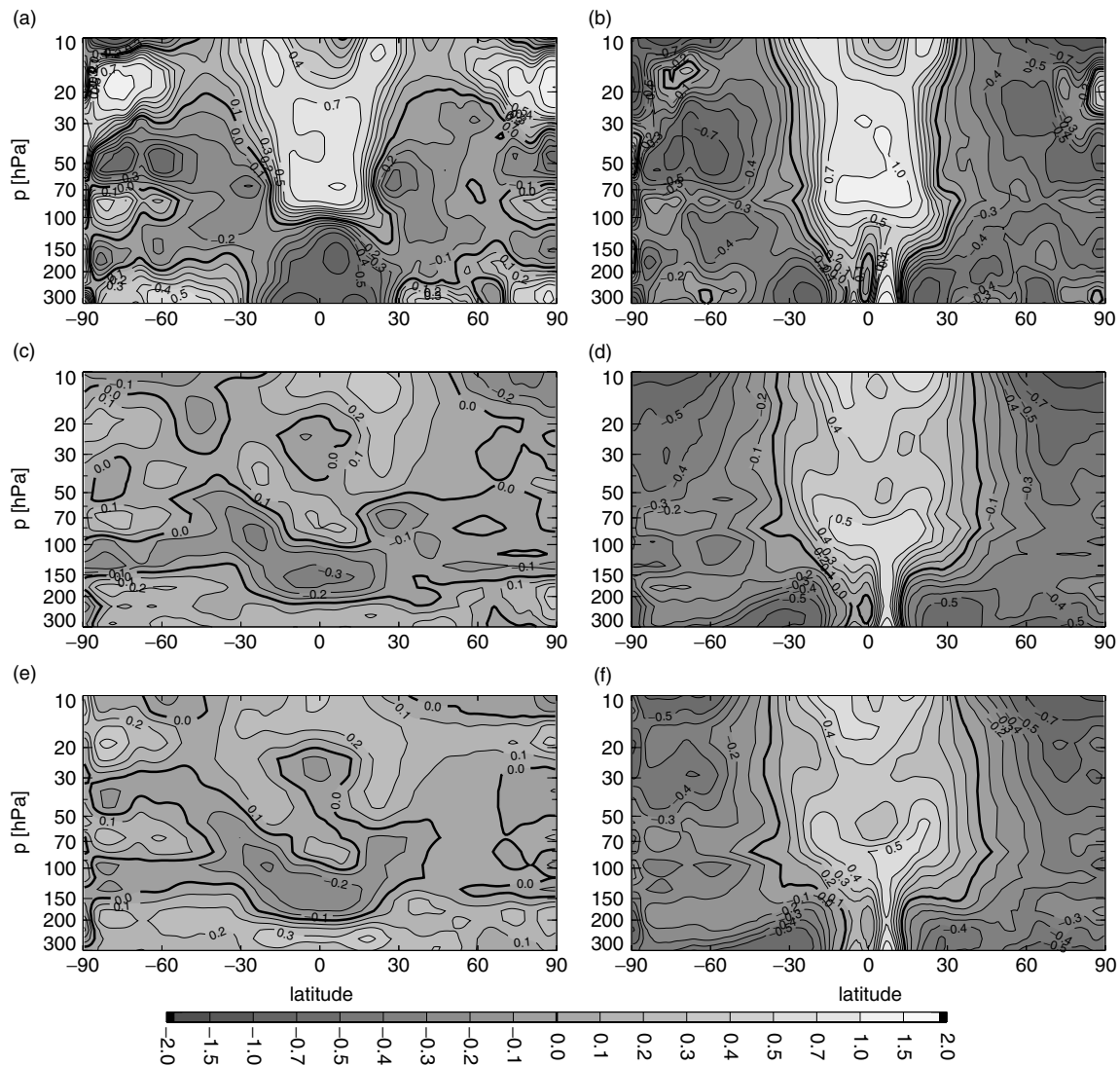
Figure 11. Annual (year 2000), zonal mean assimilation temperature increment (K day^{-1}) for (a) ERA-40, (c) EXP-471, and (e) ERA-Interim. (b), (d) and (f) show the corresponding total diabatic heating (being the sum of the model diabatic heating and the assimilation temperature increment). Note changes in contour spacing at ±0.5, ±0.7, ±1 K day^{-1}.

the comparison estimates, though this may be due to types (1) and (2) errors (the latter arising from the ozone climatology). A plausible explanation then could be that the ECMWF models overestimate radiative heating, which leads to a temperature drift over the forecast period towards too high temperatures, and subsequent correction (cooling) by the assimilation. An alternative explanation is that the convective parametrization does not properly reflect the thermal impact of very deep convection and could, perhaps, miss the cooling effect of detrainment above the level of neutral buoyancy.

In ERA-40, the entire tropical upper troposphere experiences cooling from the assimilation temperature increment, and the cooling above 200 hPa is stronger than in the two other reanalyses. Conversely, the ERA-40 model diabatic heating, in particular the contribution from latent heat release (not shown separately), is much larger (on average about 0.5 K day^{-1}, peaking at more than 1 K day^{-1} at latitudes of most frequent convection) than in the other two reanalyses. This may be interpreted as

a consequence of the previously noted excessive tropical circulation (Uppala *et al.*, 2005). Also, the cloud radiative impact is larger (more positive) in ERA-40 than in ERA-Interim, which is also consistent with too much tropical convection in ERA-40. Conversely, the positive assimilation temperature increment up to 200 hPa in ERA-Interim and EXP-471 may indicate too little latent heat release as a consequence of an underestimation of tropical convection.

5.3.2. *The stratosphere*

The total diabatic heating/cooling in the lower-latitude stratosphere shown in Figures 11(b, d, f) shows the structure and magnitudes of ERA-Interim and EXP-471 to be similar. The structure of diabatic heating in this region, in particular also the 'double peak' structure over the subtropics at about 70 hPa, is somewhat attenuated by the assimilation temperature increment, but is still clearly visible. The assimilation temperature increment

around 30 hPa induces a slight cooling over the Tropics, and a slight warming over the subtropics, such that the 'bottleneck' in the model diabatic heating at this level is removed (compare with Figure 1(b)). Upwelling now prevails between about 40°S and 40°N from about 100 hPa upwards.

For ERA-40, the assimilation temperature increment produces a strong heating in this region, and the resulting total diabatic heating is about a factor two larger than ERA-Interim or EXP-471. A warm bias in ERA-40 may be responsible for suppressed radiative heating in the lower latitude stratosphere (section 3.1). However, the magnitude of the correction from the assimilation increment is much larger than the low bias in model radiative heating rates. Hence, it is possible that ERA-40 suffers from a type (3) error in this region. The fact that ERA-Interim and EXP-471 require much smaller assimilation increments suggests that the problem may be related to the assimilation process rather than the model itself.

At high latitudes, differences in the diabatic heat budget between ERA-40 and ERA-Interim are particularly pronounced. We have shown above that the peculiar oscillatory patterns in radiative heating rates in ERA-40 are a consequence of an incorrect temperature profile, with layers that are too warm/cold having too much/little radiative cooling. The assimilation increment of ERA-40 (and to a much lesser degree in ERA-Interim) corrects for these errors (Figure 11), and the resulting total (model diabatic plus assimilation temperature increment) diabatic heating/cooling shows a more realistic structure (but note that some weaker oscillatory patterns remain).

The comparison of the total diabatic heating between ERA-40 on the one hand, and EXP-471 and ERA-Interim on the other hand, shows that the stratospheric circulation as represented by ERA-40 wind fields corresponds to a much stronger diabatic residual circulation. It is well known that stratospheric age of air calculated from analysed data may give unrealistic values (e.g. Schoeberl *et al.*, 2003), and that calculations based on ERA-40 wind fields have a strong bias towards air being too young (e.g. Scheele *et al.*, 2005; Monge-Sanz *et al.*, 2008). However, a multitude of factors may lead to such a bias, and little can be said about the diabatic residual circulation from age of air calculations alone. Characterization of stratospheric transport would thus greatly benefit from a combination of age of air calculations with the calculation of the total diabatic heating.

Overall, ERA-Interim appears to provide a much improved stratospheric temperature field, and diabatic circulation. As documented in detail by Uppala *et al.* (2005), Simmons *et al.* (2006) and Uppala *et al.* (2008), this progress resulted from various factors. Perhaps most importantly, a number of improvements in the data assimilation system have led to a smaller difference between the model background state and the state enforced by the assimilation system.

It was found that the radiative transfer calculations using the fast radiative transfer model (RTTOV) for the temperature retrieval from satellite radiances of the top three channels 12, 13 and 14 of the Advanced Microwave Sounding Unit (AMSU) employed an inaccurate modelling of the Zeeman effect (a type (1) error in our classification). For ERA-Interim, the Zeeman effect is simply removed, and the consistency between Stratospheric Sounding Unit channel 3 and AMSU channel 14 is improved. Also, it was found that in the old RTTOV the weighting function for AMSU-A channel 14 was located too high, which created problems particularly during the polar night, when the mesosphere is warmer than the stratosphere. However, the introduction of AMSU radiances still causes a temperature jump at levels higher than 10 hPa in ERA-Interim. Compared to these changes in the assimilation system, the changes brought about by the use of a 6-spectral-interval version of the short-wave radiative transfer model, leading to slightly larger radiative heating rates in the stratosphere (Figure 4(b)) are probably minor.

The changes in the data assimilation system led to a state that is closer to that of the model particularly in the upper stratosphere, with important consequences. In ERA-40, the large discrepancy led to very large assimilation increments that apparently induced temperature oscillations well down to the lower stratosphere. Because of the deep vertical structure of satellite radiances, such oscillations cannot be effectively constrained by data other than radiosondes. Indeed, we find (not shown) that the assimilation increment at radiosonde locations tries to eliminate these oscillations. However, their overall weight in the assimilation system was insufficient to correct the spurious oscillations imposed higher up.

While these problems can be understood in terms of types (1) and (2) errors, the important question about the ultimate cause of the excessive diabatic circulation in the stratosphere must remain unanswered. Only errors of type (3) induce heat fluxes that require correction by the assimilation increment that, when added to the total model diabatic heating, do not add up to the true diabatic heating. However, we could not locate a *single largest* process that may have induced the apparently large spurious heat fluxes in ERA-40.

6. Outlook

The comparison of the total diabatic heating rates of the three reanalyses illustrates our assertion given above that the average diabatic circulation in reanalyses can be very different, and that excessive heating in one place can be compensated by excessive cooling in another without violating the constraints arising from energy conservation. The results presented in this paper show that due care should be used when deducing residual circulations from (re)analyses, as the observed differences in total diabatic heating not only arise from model deficiences in diabatic heating (which would not constitute a problem for analyses of Eliassen–Palm fluxes, for example), but also due to spurious heat fluxes associated with spurious eddy (vertical and horizontal) heat fluxes. The fact that the temperature assimilation increment is much smaller in the new interim reanalyses than in ERA-40 suggests

that the diabatic heat budget in these reanalyses is much closer to reality. The improvement arises from a combination of improvements in the model, and in the assimilation system with a 4D-Var assimilation procedure and an improved correction for biases in the observations entering the assimilation system.

The comparison between ERA-Interim and ERA-40, and the analysis of the corresponding assimilation increments, show that the next generation of reanalyses can be expected to provide a fairly accurate representation of the general circulation, and in particular also of its diabatic residual circulation. Such reanalyses may then allow us to study the diabatic residual circulation, its driving processes, and variability and trends therein, with even greater accuracy, and without the need of *ad hoc* solutions to satisfy the global heat budget. Some ambiguity will remain as a result of the use of climatologies of, for example, ozone, which induces type (2a) errors that can prevent direct use of model diabatic heating for further analyses.

The progress seen between ERA-40 and ERA-Interim, in particular the much smaller assimilation increment in the latter, gives hope that, in the not so distant future, analysis data products will be of high enough quality that it may also be possible to analyse time series of the assimilation increment for signals arising from changes in the climate system that are not captured by the model. Such an analysis would provide extremely valuable information about model deficiencies affecting their ability to reliably predict climate changes.

In this work we have focussed on the diabatic terms of the thermodynamic energy equation. Questions to be addressed in future work are (i) to what extent the total diabatic heat budget (including assimilation increment) reconciles with the diabatic residual circulation determined via the transformed Eulerian mean equations, and (ii) to what extent previously published analyses in the TEM framework (based on older reanalysis and operational analyses) and data products suffer from the same deficiences that lead to the large assimilation increments seen in ERA-40.

Acknowledgements

References

Baldwin MP, Gray LJ, Dunkerton TJ, Hamilton K, Haynes PH, Randel WJ, Holton JR, Alexander MJ, Hirota I, Horinouchi T, Jones DBA, Kinnersley JS, Marquardt C, Sato K, Takahashi M. 2001. The quasi-biennial oscillation. *Rev. Geophys.* **39**: 2, 179–229.

Boville BA, Rasch PJ, Hack JJ, McCaa JR. 2006. Representation of clouds and precipitation processes in the Community Atmosphere Model Version 3 (CAM3). *J. Climate* **19**: 2184–2198.

Bresser G, Manning AJL, Pawson S, Rodgers CD. 1995. A new parameterization of scale-dependent radiative rates in the stratosphere. *J. Atmos. Sci.* **52**: 24, 4429–4447.

Cariolle D, Déqué M. 1986. Southern hemisphere medium-scale waves and total ozone disturbances in a spectral general-circulation model. *J. Geophys. Res.* **91**: D10, 825–846.

Corti T, Luo BP, Peter T, Vömel H, Fu Q. 2005. Mean radiative energy balance and vertical mass fluxes in the equatorial upper troposphere and lower stratosphere. *Geophys. Res. Lett.* **32**: L06802, DOI: 10.1029/2004GL021889.

Dima I, Wallace JM. 2007. Structure of the annual-mean equatorial planetary waves in the ERA-40 reanalyses. *J. Atmos. Sci.* **64**: 2862–2880, DOI: 10.1175/JAS3985.1.

Dunkerton T. 1978. On the mean meridional mass motions of the stratosphere and mesosphere. *J. Atmos. Sci.* **35**: 2325–2333.

Fels SB. 1982. A parameterization of scale-dependent radiative damping rates in the middle atmosphere. *J. Atmos. Sci.* **39**: 1141–1152.

Folkins I, Loewenstein M, Podolske J, Oltmans SJ, Proffit M. 1999. A barrier to vertical mixing at 14 km in the Tropics: Evidence from ozoneondes and aircraft measurements. *J. Geophys. Res.* **104**: D18, 22 095–22 102.

Fortuin JPF, Langematz U. 1994.. An update on the global ozone climatology and on concurrent ozone and temperature trends. *Proceedings SPIE Vol. 2311, Atmospheric Sensing and Modeling*, 207–216.

Fouquart Y, Bonnel B. 1980. Computation of solar heating of the Earth's atmosphere: A new parameterization. *Beitr. Phys.* **53**: 35–62.

Fu Q, Liou KN. 1993. Parameterization of the radiative properties of cirrus clouds. *J. Atmos. Sci.* **50**: 2008–2025.

Fueglistaler S, Wernli H, Peter T. 2004. Tropical troposphere-to-stratosphere transport inferred from trajectory calculations. *J. Geophys. Res.* **109**: D03108, DOI: 10.1029/2003JD004069.

Fueglistaler S, Fu Q. 2006. Impact of clouds on radiative heating rates in the tropical lower stratosphere. *J. Geophys. Res.* **111**: D23202, DOI: 10.1029/2006JD007273.

Gettelman AE, de Forster PM, Fujiwara M, Fu Q, Vömel H, Gohar LK, Johanson C, Ammerman M. 2004. Radiation balance of the tropical tropopause layer. *J. Geophys. Res.* **109**: DOI: 10.1029/2003JD004190.

Gill AE. 1980. Some simple solutions for heat-induced tropical circulation. *Q. J. R. Meteorol. Soc.* **106**: 447–462.

Goody RM, Yung YL 1989. *Atmospheric Radiation*. Oxford University Press: New York.

Hartmann DL, Moy LA, Fu Q. 2001. Tropical convection and the energy balance at the top of the atmosphere. *J. Climate* **14**: 24, 4495–4511.

Hasebe F. 1994. Quasi-biennial oscillations of ozone and diabatic circulation in the equatorial stratosphere. *J. Atmos. Sci.* **51**: 5, 729–745.

Haynes PH, Marks CJ, McIntyre ME, Shepherd TG, Shine KP. 1991. On the 'downward control' of extratropical diabatic circulations by eddy-induced mean zonal forces. *J. Atmos. Sci.* **48**: 4, 651–678.

Held IM, Hou AY. 1980. Nonlinear axially symmetric circulations in a nearly inviscid atmosphere. *J. Atmos. Sci.* **37**: 515–533.

Highwood EJ, Hoskins BJ. 1998. The tropical tropopause. *Q. J. R. Meteorol. Soc.* **124**: 1579–1604.

Holton JR, Haynes PH, McIntyre ME, Douglass AR, Rood RB, Pfister L. 1995. Stratosphere–troposphere exchange. *Rev. Geophys.* **33**: 403–440.

Jensen EJ, Toon OB, Selkirk HB, Spinhirne JD, Schoeberl MR. 1996. On the formation and persistence of subvisible cirrus clouds near the tropical tropopause. *J. Geophys. Res.* **101**: 21 361–21 375.

McFarlane SA, Mather JH, Ackerman TP. 2007. Analysis of tropical radiative heating profiles: A comparison of models and observations. *J. Geophys. Res.* **112**: D14218, DOI: 10.1029/2006JD008290.

Mlawer EJ, Taubman SJ, Brown PD, Iacono MJ, Clough SA. 1997. Radiative transfer for inhomogeneous atmospheres: RRTM, a validated correlated-k model for the longwave. *J. Geophys. Res.* **102D**: 16 663–16 682.

Monge-Sanz BM, Chipperfield MP, Simmons AJ, Uppala SM. 2008. Mean age of air and transport in a CTM: Comparison of different ECMWF analyses. *Geophys. Res. Lett.* **34**: L04801, DOI: 10.1029/2006GL02815.

Morcrette J-J. 2002. Assessment of the ECMWF model cloudiness and surface radiation fields at the ARM-SGP site. *Mon. Weather Rev.* **130**: 257–277.

Norton WA. 2006. Tropical wave driving of the annual cycle in the tropical tropopause temperatures. Part II: Model results. *J. Atmos. Sci.* **63**: 1420–1431.

Oikonomou EK, O'Neill A. 2006. Evaluation of ozone and water vapor fields from the ECMWF reanalysis ERA-40 during 1991–1999 in comparison with UARS satellite and MOZAIC aircraft observations. *J. Geophys. Res.* **111**: D14109, DOI: 10.1029/2004JD005341.

Pawson S, Stajner I, Kawa SR, Hayashi H, Tan WW, Nielsen JE, Zhu Z, Chang LP, Livesey NJ. 2007. Stratospheric transport using 6-hour-averaged winds from a data assimilation system. *J. Geophys. Res.* **112**: D23103, DOI: 10.1029/2006JD007673.

Peixoto JP, Oort AH. 1992. *Physics of Climate*. American Institute of Physics: New York.

Plumb RA, Eluszkiewicz J. 1999. The Brewer–Dobson circulation: Dynamics of the tropical upwelling. *J. Atmos. Sci.* **56**: 868–890.

Rosenfield JE, Considine DB, Schoeberl MR, Browell EV. 1998. The impact of subvisible cirrus clouds near the tropical tropopause on stratospheric water vapor. *Geophys. Res. Lett.* **25**: 11, 1883–1886.

Rosenlof KH. 1995. Seasonal cycle of the residual mean meridional circulation in the stratosphere. *J. Geophys. Res.* **100**: D3, 5173–5191.

Scheele MP, Siegmund PC, van Velthoven PFJ. 2005. Stratospheric age of air computed with trajectories based on various 3D-Var and 4D-Var data sets. *Atmos. Chem. Phys.* **5**: 1–7.

Schoeberl MR. 2004. Extratropical stratosphere–troposphere mass exchange. *J. Geophys. Res.* **109**: D13303, DOI: 10.1029/2004JD004525.

Schoeberl MR, Douglass AR, Zhu Z, Pawson S. 2003. A comparison of the lower stratospheric age spectra derived from a general circulation model and two data assimilation systems. *J. Geophys. Res.* **108**: D3, 4113, DOI: 10.1029/2002JD002652.

Sherwood SC. 2000. A stratospheric 'drain' over the Maritime Continent. *Geophys. Res. Lett.* **27**: 5, 677–680.

Simmons A, Uppala S, Dee D, Kobayashi S. 2006. 'ERA-Interim: New ECMWF reanalysis products from 1989 onwards'. *ECMWF Newsletter* **110**: 25–35.

Spang R, Eidmann G, Riese M, Offermann D, Preusse P, Pfister L, Wang PH. 2002. CRISTA observations of cirrus clouds around the tropopause. *J. Geophys. Res.* **107**: D23, DOI: 10.1029/2001JD000698.

Sprenger M, Maspoli MC, Wernli H. 2003. Tropopause folds and cross-tropopause exchange: A global investigation based upon ECMWF analyses for the time period March 2000 to February 2001. *J. Geophys. Res.* **108**: D12, 8518, DOI: 10.1029/2002JD002587.

Tan WW, Geller MA, Pawson S, da Silva A. 2004. A case study of excessive subtropical transport in the stratosphere of a data assimilation system. *J. Geophys. Res.* **109**: D11102, DOI: 1029/2003JD004057.

Thompson AM, Witte JC, McPeters RD, Oltmans SJ, Schmidlin FJ, Logan JA, Fujiwara M, Kirchhoff VWJH, Posny F, Coetzee GJR, Hoegger B, Kawakami S, Ogawa T, Johnson BJ, Vömel H, Labow G. 2003. Southern Hemisphere Additional Ozonesondes (SHADOZ) 1998–2000 tropical ozone climatology. 1. Comparison with Total Ozone Mapping Spectrometer (TOMS) and ground-based measurements. *J. Geophys. Res.* **108**: D2, 8238, DOI: 10.1029/2001JD000967.

Trenberth KE, Stepaniak DP. 2003. Seamless poleward atmospheric energy transports and implications for the Hadley circulation. *J. Climate* **16**: 3706–3722.

Uppala SM, Kållberg PW, Simmons AJ, Andrae U, Da Costa Bechtold V, Fiorino M, Gibson JK, Haseler J, Hernandez A, Kelly GA, Li X, Onogi K, Saarinen S, Sokka N, Allan RP, Andersson E, Arpe K, Balmaseda MA, Beljaars ACM, Van de Berg L, Bidlot J, Bormann N, Caires S, Chevallier F, Dethof A, Dragosavac M, Fisher M, Fuentes M, Hagemann S, Hólm E, Hoskins BJ, Isaksen L, Janssen PAEM, Jenne R, McNally AP, Mahfouf JF, Morcrette J-J, Rayner NA, Saunders RW, Simon P, Sterl A, Trenberth KE, Untch A, Vasiljevic D, Viterbo P, Woollen J. 2005. The ERA-40 re-analysis. *Q. J. R. Meteorol. Soc.* **131**: 2961–3012.

Uppala S, Dee D, Kobayashi S, Berrisford P, Simmons A. 2008. 'Towards a climate data assimilation system: Status update of ERA-Interim'. *ECMWF Newsletter* **115**: 12–18.

Wang PH, Minnis P, McCormick MP, Kent GS, Skeens KM. 1996. A 6-year climatology of cloud occurrence frequency from Stratospheric Aerosol and Gas Experiment II observations (1985–1990). *J. Geophys. Res.* **101**: (D23), 29 407–29 429.

Winker DM, Trepte CR. 1998. Laminar cirrus observed near the tropical tropopause by LITE. *Geophys. Res. Lett.* **25**: 3351–3354.